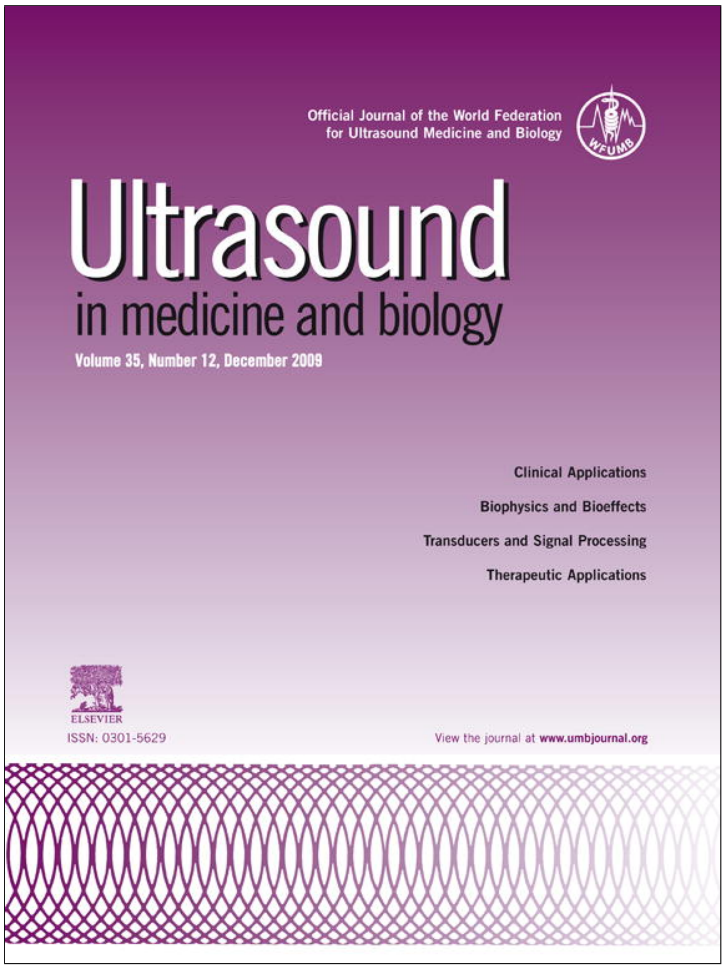

Ultrasound in Med. & Biol., Vol. 35, No. 12, pp. 1995–2006, 2009

0301-5629/09/$–see front matter

ELSEVIER

doi:10.1016/j.ultrasmedbio.2009.05.019

● *Original Contribution*

# ULTRASOUND PHASE CONTRAST THERMAL IMAGING WITH REFLEX TRANSMISSION IMAGING METHODS IN TISSUE PHANTOMS

CALEB H. FARNY and GREGORY T. CLEMENT
Department of Radiology, Harvard Medical School, Brigham and Women's Hospital, Boston, MA

(*Received* 11 *December* 2008, *revised* 16 *April* 2009, *in final form* 25 *May* 2009)

**Abstract—Thermal imaging measurements using ultrasound phase contrast have been performed in tissue phantoms heated with a focused ultrasound source. Back projection and reflex transmission imaging principles were used to detect sound speed–induced changes in the phase caused by an increase in the temperature. The temperature was determined from an empirical relationship for the temperature dependence on sound speed. The phase contrast was determined from changes in the sound field measured with a hydrophone scan conducted before and during applied heating. The lengthy scanning routine used to mimic a large two-dimensional array required a steady-state temperature distribution within the phantom. The temperature distribution in the phantom was validated with magnetic resonance (MR) thermal imaging measurements. The peak temperature was found to agree within 1°C with MR, and good agreement was found between the temperature profiles. The spatial resolution was 0.3 × 0.3 × 0.3 mm, comparing favorably with the 0.625 × 0.625 × 1.5-mm MR spatial resolution.**
**(E-mail: cfarny@bwh.harvard.edu)** 

*Key Words:* **Thermometry, Phase contrast imaging, Reflex transmission imaging.**

## INTRODUCTION

A number of applications exist for noninvasive temperature sensing in tissue, including tissue characterization, perfusion imaging and, perhaps most notably, thermal therapy procedures. Magnetic resonance (MR) imaging remains the current gold standard (Quesson et al. 2000; McDannold 2005) by measuring the proton resonant frequency shift to determine temperature change with adequate temporal and spatial resolution. The associated expense, accessibility challenges, and portability have provided motivation for continued investigation of alternative methods, such as microwave radiometry (Meaney et al. 2003), impedance tomography (Paulsen et al. 1996), and various ultrasound techniques (Simon et al. 1998; Miller et al. 2004; Farny and Clement 2008). Ultrasound is an attractive modality for thermal imaging because it is noninvasive, nonionizing and relatively inexpensive and portable. Here we report on continuing efforts for applying an ultrasound phase-contrast method in a pulse-echo arrangement for imaging ultrasound–induced temperature change.

Address correspondence to: Dr. Caleb. H. Farny, Department of Radiology, Harvard Medical School, Brigham and Women's Hospital, Boston, MA 02115. E-mail: cfarny@bwh.harvard.edu

The use of ultrasound as a tissue thermometer has spurred investigation of the temperature dependence of various acoustic properties for multiple tissue types. Attenuation (Damianou et al. 1997), the nonlinearity parameter $B/A$ (Liu et al. 2008) and phase speed (Bamber and Hill 1979; Duck 1990) have all been documented to exhibit a dependence on temperature. The underlying goal is to be able to measure in a clinical setting where acoustic window access may be limited and calibrate the dependence to exploit these relationships for determination of either the absolute temperature or temperature change. The utility of acoustic properties depends on the application and accompanying temperature range of interest. For example, Damianou et al. (1997) found that attenuation and absorption in *in vitro* dog muscle, liver, and kidney increased from 50–65°C, but otherwise exhibited little change for lower temperatures. These findings were in agreement with similar studies by Robinson and Lele (1972), Bamber and Nassiri (1985) and Worthington and Sherar (2001). This relationship would not necessarily be helpful for measurements that rely on small temperature differences near body temperature but could prove effective for thermal ablation monitoring (Clarke et al. 2003; Tyreus and Diederich 2004). The nonlinearity parameter appears to have a linear dependence on temperature, as demonstrated by Liu et al. (2008)

for *in vitro* porcine fat and liver samples. Results for temperatures up to 45°C agreed well with thermocouple measurements. This method has only recently been achieved for pulse-echo arrangements (Gong et al. 2004), a major barrier for many ultrasound-based methods.

The temperature dependence of sound speed has been investigated for a number of tissue types (Bamber and Hill 1979; Duck 1990), revealing variation between tissue type, especially depending on fat content. Most nonfatty tissues exhibit increasing sound speeds for temperatures up to 50–65°C, followed by a decreasing slope at higher temperatures. Fatty tissues instead exhibit a negative slope. These relationships have been used in numerous studies seeking to use sound speed as an indicator of temperature. A common approach has been to use a diagnostic ultrasound imaging platform, where the radiofrequency (RF) data obtained with a standard imaging array before and after heating are compared. The assumption of a uniform sound speed by the imaging system results in a spatial shift in the image because of the variation in sound speed when the tissue is heated. This method has been pursued using various cross-correlation techniques (Maass-Moreno et al. 1996; Simon et al. 1998; Miller et al. 2004; Pernot et al. 2004; Anand et al. 2007) that have been successful in measuring temperature rises up to 15°C in *in vitro* tissue. Varghese et al. (2002) obtained *in vivo* images of heat from a RF applicator up to 100°C using 2-D cross-correlation methods, although the ultrasound-derived temperature was not compared directly with thermocouple data. More recently, Daniels et al. (2007) demonstrated good agreement of RF-induced temperature change (23 to 65°C) in tissue phantoms when a 2-D correlation-based method was compared with implanted fiber optic thermocouples. The analysis involved use of a linear relationship between the measured sound speed shift and temperature rise throughout the entire temperature range (40 to 100°C), despite the nonmonotonic sound speed–temperature relationship exhibited in many nonfatty tissues. The study rationalized that the linear relationship was effective because of the additional effect of thermal expansion exhibited in these tissues, a parameter that also exhibited a larger percent variation than sound speed over the temperature range of interest.

We recently reported a study for measuring temperature change with ultrasound based on phase contrast and back projection methods in a through-transmission arrangement (Farny and Clement 2008). A thermal plume in water and a tissue phantom were both used to approximate a steady-state phase contrast scenario, where the phase difference was the result of a change in sound speed in the medium. A focused transducer interrogated the medium and the sound field was mapped with a needle hydrophone scan, before and after the phase contrast was present along the interrogation path. The measured fields were back-projected and the phase change between the two fields was used to determine the temperature change using an empirical relationship between sound speed and temperature in water. This approach differs from cross-correlation methods in that phase measurements have low sensitivity to noise and do not rely on speckle tracking, which may introduce error if the speckle signal does not originate from the region-of-interest (ROI). The study built on earlier preliminary experimental and simulation studies by King et al. (2003) and Clement and Hynynen (2005), respectively, that used phase contrast methods for measuring temperature change in soft tissue. King et al. used an acoustic array camera in through-transmission mode to monitor cooling in rabbit tissue after ultrasound-induced heating. The image intensity was found to correlate with temperature because of the change in sound speed. Clement and Hynynen studied the effect more closely by examining the use of phase imaging to measure temperature rise in simulated muscle and fat tissue. The technique found that in the presence of Gaussian noise, a signal-to-noise ratio (SNR) as low as 1.1 dB in breast and 2.9 dB in fat tissue was sufficient to resolve the temperature rise. This sensitivity compares favorably with MR, which for proton resonant frequency shift-based thermal imaging requires a SNR of at least 7 dB (Palussière et al. 2003), and up to 100 dB for optimal temperature variance (Rieke and Pauly 2008). These sensitivities are significantly lower than the minimum required SNR of 20 dB reported by Miller et al. (2002) for their simulation of an ultrasound echo-strain thermal imaging method, although future improvement in signal processing methods may help increase sensitivity.

In an effort to extend these techniques towards a clinically-oriented measurement, we have performed a study that uses reflex transmission imaging (RTI) techniques to measure ultrasound-induced heating in tissue phantoms. RTI has been used to improve attenuation-based images in gall and kidney stone (Green and Arditi 1985; Green et al. 1991) and skin lesion (Rallan et al. 2007) imaging. In these studies, the backscattered signals emanating from beyond the focus of an imaging transducer were used to provide an illuminating source signal that would be affected by the propagation characteristics within the focal zone. Because the RTI signal reflects off the tissue structure positioned distal to the ROI, it acts as a virtual source that transmits through the entire region. The backscattered signal was windowed and integrated, producing an image that had poor axial resolution but was strongly influenced by the attenuation within the focus. In this study, we applied the same concept of using a backscattered signal to illuminate the ROI, where instead of attenuation contrast we relied on sound speed contrast because of heating along the path. A focused

transducer was used to create a steady-state temperature rise in a tissue-mimicking phantom, and a back projection method was used to determine the phase angle throughout the ROI. Because of the lengthy measurement time, we were constrained to measuring steady-state heating in tissue phantoms. Nonetheless, the method is shown to have good agreement with temperature measurements obtained with MR thermal imaging techniques.

*Theory*

The wave equation for planar wave propagation may be solved by $P(z,t) = A\ \exp(-i\omega(t-z/c))$, where $P$ is the pressure, $A$ is the amplitude, $i$ is the complex imaginary number, $\omega$ is the angular frequency, $t$ is the time, $z$ represents distance and $c$ is the phase speed. We assume that we know these parameters for a medium in a reference state, *i.e.*, before inducing heating, particularly with regards to the phase speed. Characterization of the phantom used in these measurements provided the reference phase speed, and we note that a CT scan for nonhomogeneous media such as tissue may be applied to identify tissue type, from which the position-dependent phase speed may be identified. We further assume that the only parameter affected by a temperature change will be the phase speed, allowing the following relationship for the change in phase angle $\Phi$ over a distance $z$ to be defined:

$$\Delta\phi = \phi_{heat} - \phi_{ref} = \omega z\left(\frac{1}{c_{heat}} - \frac{1}{c_{ref}}\right). \quad (1)$$

Thus, by comparing the change in phase angle, the change in sound speed may be determined.

Given knowledge of the medium parameters in its reference state, we may obtain the phase angle at any position in the measurement space *via* implementation of planar propagation methods (Stepanishen and Benjamin 1982). Numerical propagation of the pressure field $P_0$ from its initial $x$-$y$ plane at position $z_0$ to the new position $z_i$ can be performed by first applying a 2-D Fourier transform to the pressure field $P_0(x,y,z_0)$. Working in the wave vector space, where $k_x$ and $k_y$ are the wave numbers along the $x$ and $y$ axes, the field may be propagated by multiplying by a propagation operator and performing the 2-D inverse Fourier transform, as described by

$$P_i(x,y,z_i) = \frac{1}{2\pi}\iint P_0(k_x,k_y,z_0) \exp\left(i(z_0 - z_i)\sqrt{\frac{\omega^2}{c^2} - k_x^2 - k_y^2}\right) dk_x dk_y,$$

where $P_i$ is the pressure field located at the $x$-$y$ plane at position $z_i$. For this operation, it is necessary to adequately measure the pressure field-of-interest with sufficient spatial resolution to satisfy the Nyquist spatial sampling frequency, as defined by the imaging frequency and the low-pass spatial frequency cutoff of $k_x^2 + k_y^2 = \frac{\omega^2}{c^2}$. The interrogation field for the reference and heated cases was projected back through the region of heating, allowing the phase angle throughout the region volume to be determined.

Reflex transmission imaging refers to the concept that for a sound field that has propagated through a region-of-interest, the field reflected off tissue structure positioned *beyond* the ROI may be thought of as a virtual source that will propagate back through the same region. The approach is illustrated in Fig. 1, where a therapy transducer heats up a tissue volume and an interrogation pulse from a diagnostic transducer reflects off the tissue region distal to the heated region. This interrogation field will be affected by the propagation effects along its path, such as a shift in the phase speed because of elevated temperatures. Using these concepts, a reflex transmission image was created that showed the heating in the imaging plane. The fields measured with the hydrophone were projected approximately 5 mm through water to the phantom interface. In the phantom, the fields were projected in 1-mm steps until the axial position corresponding to the therapeutic focus was reached and the phase difference between the fields at each axial position was determined. The cumulative heating effects were obtained by integrating the phase difference along the projection axis.

The integrated phase difference provides the heating effects along the imaging plane ($x$-$y$, following the orientation in Fig. 2). In the current study, the temperature change along the imaging ($z$) axis was obtained by assuming the heating profile is axi-symmetric, such that the profile along the $z$-axis is similar to that along the

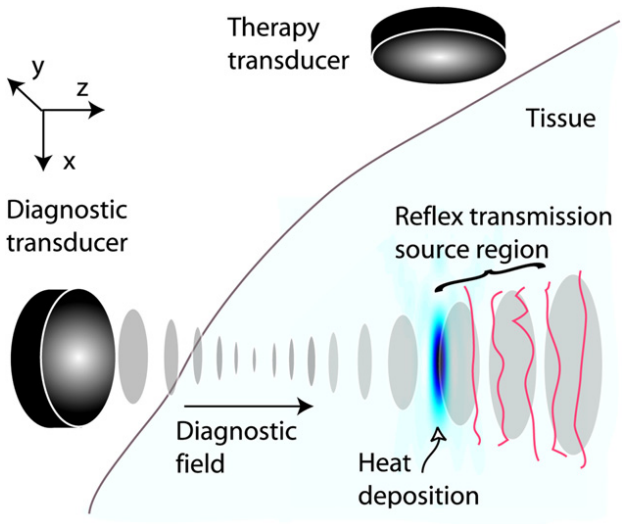


Fig. 1. Illustration of the reflex transmission imaging (RTI) principle.

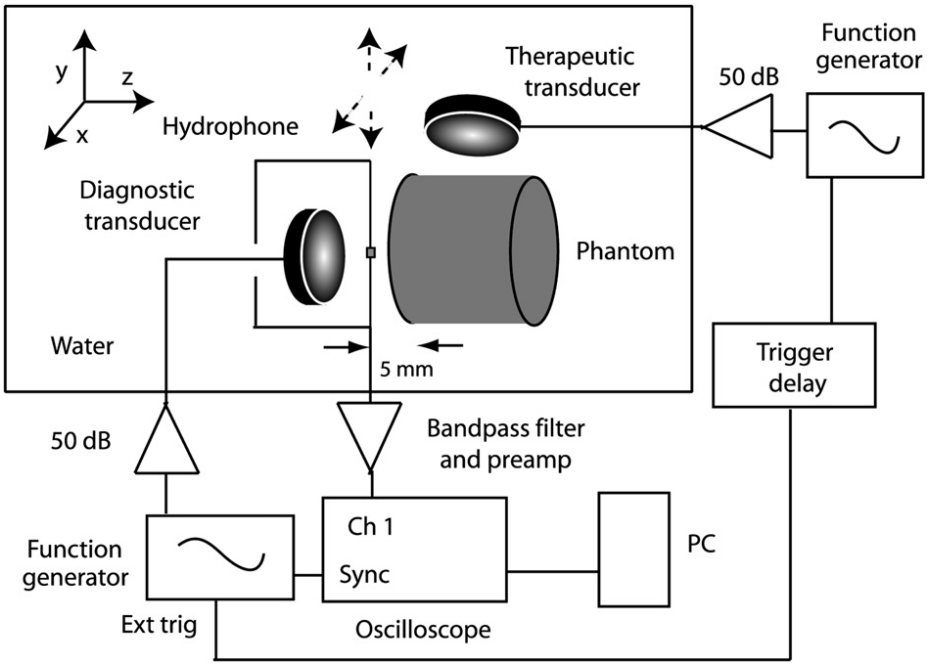


Fig. 2. Experimental arrangement.

vertical ($y$) axis, and neglecting thermal refraction effects. The profile along the $z$-axis may then be obtained by applying the Fourier slice theorem, which states that a Fourier transform of a projection along an angle is equivalent to a slice through the origin in wave vector space (Kak and Slaney 1988). The axi-symmetric condition allows the slice to represent the phase at all other angles through the origin in wave vector space. This was applied by performing a Fourier transform on the phase difference along the $y$-axis at a given lateral $x$ position, rotating it about the origin in wave vector space, and performing a 2-D inverse Fourier transform.

## MATERIALS AND METHODS

The experimental arrangement is shown in Fig. 2. Two focused transducers were perpendicularly aligned in a tank filled with deionized water for the separate purpose of imaging and heating a tissue-mimicking phantom. A 1.088-MHz single-element lead zirconate titanate (PZT-4) piezoceramic transducer (50-mm diameter, 100-mm radius of curvature) that was constructed and impedance matched in-house was used as the ''therapy'' transducer. The driving signal was supplied by a function generator (model 396, Fluke Corp., Everett, WA, USA), which was amplified (model 3100, ENI Corp., Rochester, NY, USA) and impedance-matched to the transducer. The ''imaging'' transducer consisted of a custom 14-ring annular PZT array, of which only the inner six rings were driven, synchronously, at its nominal 1.68-MHz center frequency, resulting in a 21-mm outer diameter and 100-mm radius of curvature. A second function generator (model 33250, Agilent Technologies Inc., Santa Clara, CA, USA) supplied the 15-cycle signal that was amplified (model 240L, E and I Ltd, Rochester, NY, USA) and triggered externally by the therapy pulse function generator. The therapy transducer was positioned such that its focus coincided with the imaging transducer acoustic axis, approximately 135 mm from the imaging transducer.

The heat distribution in the phantom was measured for two separate duty cycles to evaluate the analysis for two different temperature rises. The higher duty cycle (43%) excitation supplied to the therapy transducer consisted of a 600-cycle burst at a 790-Hz pulse repetition frequency (PRF), whereas the lower duty cycle (18%) consisted of a 200-cycle burst at 1-kHz PRF. The spatial peak temporal average intensity for continuous-wave excitation was 18 W/cm$^2$ for both excitation protocols, where the intensity was evaluated with an absorbing radiation force balance setup, as described in Sokka et al. (2003). The imaging pulse trigger was appropriately delayed using the function generator (Agilent) to prevent concurrent arrival of the imaging and therapy pulses at the hydrophone.

The sound field reflected off the phantom structure was measured with a custom-built hydrophone positioned between the imaging transducer and phantom. The hydrophone was designed to be sensitive to the reflected signals but also impose minimal impact on the outgoing sound field, because it was necessarily positioned in the imaging transducer transmit path. The hydrophone consisted of

a 1 × 1-mm polyvinyl difluoride (PVDF) sheet mounted to a 550-$\mu$m nylon wire; the sensing element size was not ideal and contributed to spatial averaging, but smaller sizes proved difficult to construct. The signal was transmitted through a 44-gauge coaxial cable and amplified with a custom bandpass filter ($f_0$ = 1.68 MHz) and preamplifier circuit, the output of which was digitized (25 Msamples/s, 8-bit, TDS 210, Tektronix Inc., Richardson, TX, USA) and recorded on a personal computer. The hydrophone was mounted to a three-axis computer-controlled positioning system (VP9000, Velmex, Inc., Bloomfield, NY, USA) that moved the hydrophone in a raster pattern along the *x-y* plane (56 × 56 mm, 0.3-mm stepsize, where $\lambda/2$ = 0.44 mm). The hydrophone was positioned 5 mm from the phantom and the scan was centered about the diagnostic transducer acoustic axis.

The tissue phantom (Ryan and Foster 1997) used in these measurements was constructed from agar and water, where propanol and silicon dioxide particles (99% <10 $\mu$m) were added to mimic the sound speed and attenuation, respectively, found in soft tissue. This particular phantom was chosen in part because of its compatibility with MR imaging; similar results using the RTI method were observed when graphite particles, which induce MR artifacts, were used for attenuation matching in place of silica. The phantom was cast in a cylindrical mold that provided a 100-mm diameter and 40-mm length. The phantom was positioned along the imaging transducer axis, with the front face approximately 115 mm from the imaging transducer. Ideally, the measurement media would have included *in vitro* tissue but the two hydrophone scans took approximately 24 h to complete, at which point it was not anticipated the tissue would have been viable.

For the analysis, it was necessary to understand the relationship between sound speed and temperature in the phantom. This relationship was measured with a through-transmission setup that used two transducers (V303, Panametrics-NDT Corp., Waltham, MA, USA) positioned bistatically in a tank filled with deionized and degassed water. Six phantoms consisting of differing lengths were individually positioned between the transducers. The transmit transducer was excited in a similar manner as the imaging transducer by a 1.088-MHz, 15-cycle pulse and the receive transducer signal was digitized (Tektronix) at 50 Msamples/s. The temperature in the tank was controlled with an immersion heater (Thermomix B, B. Braun Melsungen AG, Melsungen, Germany) and the burst transmission time was evaluated from 25–50°C in 5°C steps; maximum immersion temperatures for the transducers limited evaluation at higher temperatures. The sound speed was determined by dividing the difference in sample length with the corresponding difference in transmission time as determined with a cross-correlation routine (Hein and O'Brien 1993). Results from the three phantom pairs were averaged and are plotted as a function of temperature in Fig. 3. The temperature as a function of sound speed was fit to a third-order polynomial and this fit was used in the analysis to determine the temperature from the sound speed.

*Validation*

The results obtained with the RTI method were compared with a MR thermometry method for validation purposes. The phantom and therapy transducer were positioned in a 3 T clinical scanner (0.625 × 0.625 × 1.5 mm voxel size, GE) in an arrangement similar to the RTI measurement setup. Using multiple phantoms to accommodate both duty cycles, the phantom was sonicated using the same excitation sequence and instruments as used for heating the phantom in the RTI measurements. The phantom was sonicated for 9 min and MR images were acquired every 2.6 s; after 9 min it was deemed to have obtained a steady-state heat distribution similar to that present during the RTI measurements. For MR temperature imaging, phase-difference images of a fast spoiled gradient echo sequence were obtained to estimate changes in the temperature-sensitive water proton resonant frequency (Ishihara et al. 1995). The following parameters were used: TR/TE: 31/20 ms; flip angle: 30°; field-of-view: 10 cm; matrix (frequency × phase): 256 × 128; bandwidth: ±7.6 kHz. A time-series of images were obtained in a single plane oriented along the direction of the ultrasound beam. The scanner reconstructed complex image data needed to create these phase-difference images, which were converted to temperature maps using a temperature sensitivity of –0.01 ppm/°C (Hindman 1966).

*Signal processing*

The hydrophone RF signal was windowed in time to digitize the signals that represented reflections off the phantom structure. An example of a typical hydrophone

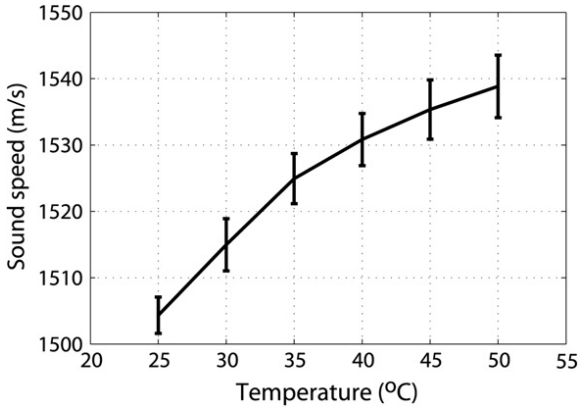


Fig. 3. Speed of sound as a function of temperature in the tissue phantom.

signal acquired in an RTI measurement is displayed in Fig. 4. Present in the signal is the reflection from the front face of the phantom, followed by scattering off the particles and the reflection off the phantom back surface. Because of minimal electrical shielding of the hydrophone cabling, the hydrophone was also sensitive to electrical noise, which included any signals that were reflected back to the imaging transducer and subsequently converted to an electrical signal. Accordingly, this aspect affected the relative positions of the transducers, hydrophone and phantom to reduce the electrical signals that were present in the time window of interest.

After the hydrophone scan, the RF signal was analyzed for the magnitude and phase of the entire reflected field over a sliding time window, from the portion of the signal extending from after the front surface reflection to the back surface reflection. The RTI measurement was evaluated using two different approaches for the reflex signal origin, the reflection off the phantom back surface and backscattering off the phantom structure; we attribute the silica particles to be the main cause of scattering in the second case. Of these two signal types, the back surface reflection provided a stronger SNR ratio, so the bulk of the results presented here are based on this signal. The second signal was investigated to demonstrate that the phase contrast RTI method is feasible in the more likely scenario where a strong planar reflector will not be present in the medium.

The sound field obtained from the sliding time window was back-projected through the phantom to the position corresponding to the maximum temperature; we assumed this point corresponded to the therapy transducer acoustic axis. The phase difference between the heated and reference fields was determined and integrated through the region of heating. For the back surface reflection, we assumed a symmetric, Gaussian distribution for the temperature profile along the imaging propagation axis. As discontinuities in the phase were occasionally present because of phase unwrapping errors, the phase difference along the vertical $y$-axis was conditioned with a 10-point smoothing average filter, and a Gaussian fit was applied to the phase difference. The phase difference fit was transformed to wave vector space and the tomographic reconstruction was applied by spinning the 1-D signal about the origin to obtain a 2-D distribution of the spatial Fourier transform. The signal was inverse transformed and the sound speed was determined using eqn (1).

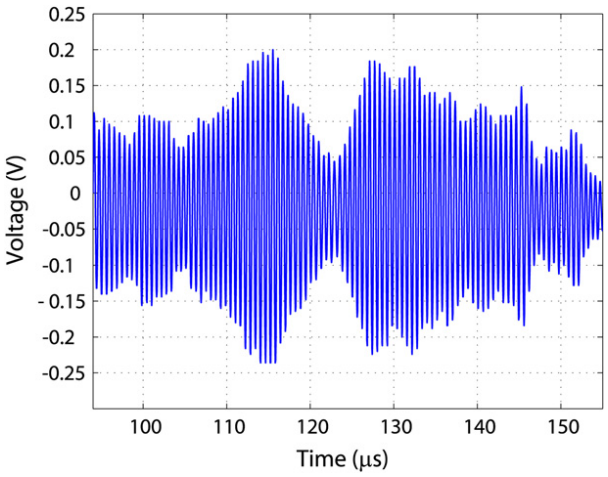


Fig. 4. Example of a typical hydrophone RF signal, where the front surface of the phantom is located at approximately 93 $\mu$s and the back surface is located at approximately 145 $\mu$s.

For the backscattered reflections, the tomographic reconstruction was not necessary. In this case, the sound field that was backscattered from each position within the sliding time window was back-projected to the point of maximum temperature. Here we hypothesized that each of these back-projected fields represented increasing degrees of exposure to the elevated temperature before they were scattered back to the hydrophone, as opposed to the back surface reflection which was assumed to have been exposed to the entire region of elevated heat on both the transmission and reflection paths. The assumption of a symmetric, Gaussian temperature profile along the $z$-axis was not necessary for the backscattered reflection approach, which relies on sufficient scattering along the entire imaging path to provide a signal of sufficient amplitude for back-projection. The peak phase difference determined for each position within the time window series represented the cumulative heating that each particular reflected field experienced by the time it propagated back to the hydrophone. The change between the cumulative phase difference at each position resulted in the phase difference that corresponded to each particular position along the $z$-axis. The sound speed was then determined as in the back surface reflection case by using eqn (1).

## RESULTS

The RTI image of the phase as a function of position within the imaging plane for the 43% duty cycle heating is displayed in Fig. 5. The field used in this result was that reflected off the back surface of the phantom, which ensured that the field was exposed to the entire region of heating. The therapy transducer was positioned along the $x$-axis, corresponding to $y = 0$, $x = -100$ mm, so that the geometric focus of the therapy transducer was at the origin of the image plane in Fig. 5. Visible in the image is an increase in the phase difference, centered about the $y$-axis at $y = 0$ mm, which drops off in amplitude with distance from $y = 0$. Referencing the relationship in eqn (1), the phase difference is expected to increase with an

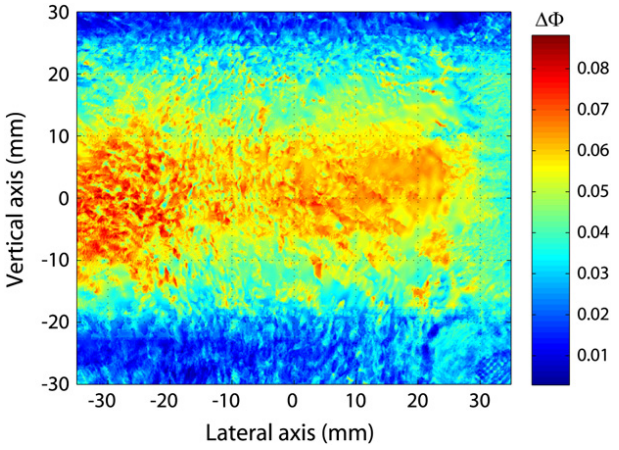


Fig. 5. RTI phase difference image of heating induced with the 43% duty cycle, where the reflex transmission field was reflected off the phantom back wall. The coordinates are relative to the imaging tranducer frame, with the therapy transducer position corresponding to $x = -100$ mm, $y = 0$ mm and the therapy transducer focus corresponding to the origin.

increase in sound speed, providing a first-order check that the phase change shown in Fig. 5 is as expected.

In comparison, the temperature rise measured with the MR method is shown in Fig. 6. The MR image plane is shown in a similar frame as the RTI image plane, and the therapy transducer was positioned parallel to the $x$-axis, with the focus at the origin, similar to the arrangement shown in Fig. 5. Qualitatively, Fig. 6 is similar to Fig. 5. The temperature rise is highest along the $y$-axis at $y = 0$ mm, as expected, and peaks at $x \sim -20$ mm. Also present in the upper portion of the image is noise in the water surrounding the phantom, as well as sporadic noise near $x = 20$, $y = -28$ mm.

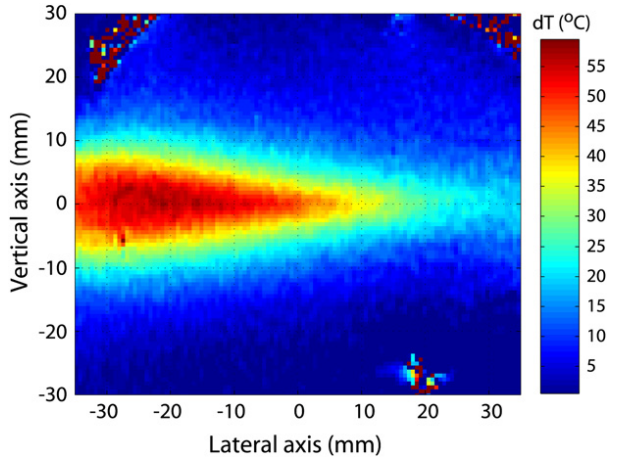


Fig. 6. Temperature rise induced in the phantom measured from the proton resonant frequency shift using MR imaging. The therapy transducer position corresponds to $x = -100$ mm, $y = 0$ mm and the therapy transducer focus is positioned at the origin.

The temperature rise measured with the MR method is compared with that determined with the RTI method in Fig. 7. The data is from the focus ($x = 0$) along the $y$-axis. The peak temperature rise measured with the RTI method was 43°C. Despite some differences in the width of the distribution, the two curves are in good agreement overall, with a difference in peak temperature of 0.5°C between the two methods. In particular, the temperature determined with the RTI method is slightly higher within ±10 mm of the peak temperature.

Although the signal amplitude was highest for the reflections off the phantom back surface, the particles in the phantom provided sufficient backscattered signal strength to allow the field to be back-projected. An example of a RTI image reconstructed from backscattering within the phantom is shown in Fig. 8. This particular field is estimated to have reflected from the position corresponding to 7 mm from the back surface of the phantom. The image is similar to Fig. 5 but with a lower amplitude phase change, as expected, because of the lower exposure to heat in the phantom; for comparison purposes, note that the amplitude scale matches that of Fig. 5. The backscattered RF signal was windowed every 2 $\mu$s and the field within each window was analyzed for the integrated phase change. The temperature corresponding to the peak phase difference at the origin for each RTI field was determined, providing the temperature along the $z$-axis (the diagnostic transducer acoustic axis). Only a portion of the signal was available for analysis, because of electronic noise present in the unshielded hydrophone RF signal in the extent corresponding to the proximal

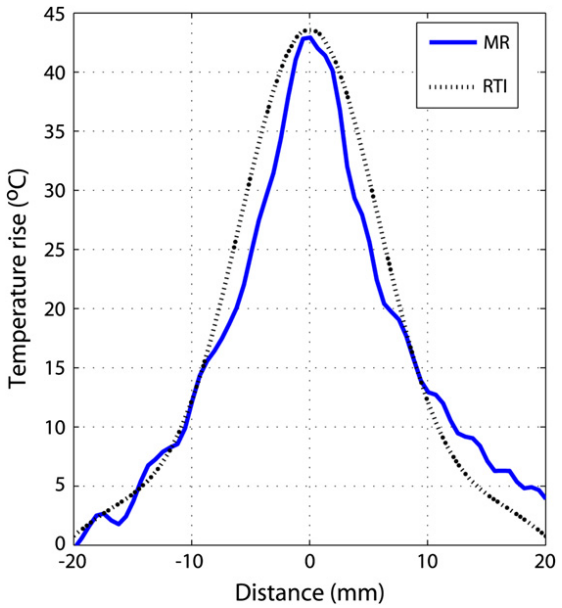


Fig. 7. The temperature rise measured with the MR and RTI technique across the therapy transducer focus ($x = 0$ mm) during the 43% duty cycle sonication.

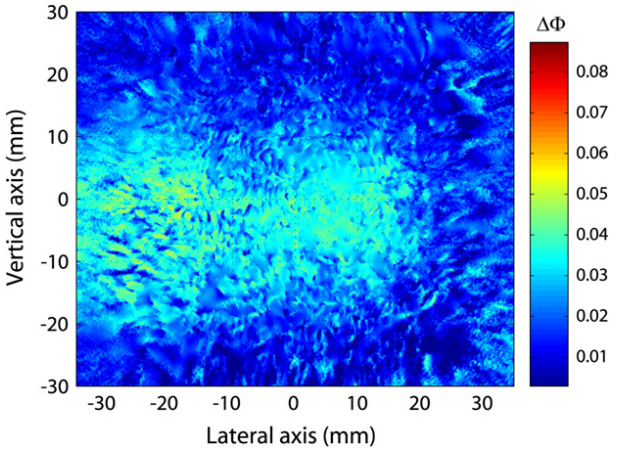


Fig. 8. RTI phase difference image based on backscattering off the particulate scatterers in the phantom during the 43% duty cycle sonication.

region of the phantom. The temperature rise determined from the remaining signal is compared with the validation temperature in Fig. 9, where the MR temperature curve was from the vertical temperature distribution. The horizontal error bars represent error in the axial position, stemming from uncertainty in the position because of the duration of the time window over which each backscattered field was evaluated. In general, the two curves are in good agreement, despite some deviation with regards to the spatial position of the temperature rise.

The RTI phase difference for the 18% duty cycle is shown in Fig. 10. Discontinuities as a result of phase unwrapping errors are evident in the periphery of the diagnostic beam (*e.g.*, $x$, $y = -5$, $-25$ mm). Despite this issue, the temperature distribution is similar to Fig. 5, where the highest phase difference is along the therapeutic transducer acoustic axis, approximately 22 mm prefocal, where the therapy transducer focus is again positioned at the origin. The RTI image may be compared with the MR temperature map shown in Fig. 11. The temperature distribution is similar to the higher-duty cycle case, and general agreement can be seen with the RTI image, where the temperature peaks at $x \sim -25$ mm. The temperature reconstructed from the RTI phase difference at the focus is compared with the temperature measured with the MR method along the focus in Fig. 12. The temperature peaked at approximately 14°C and the two methods were within 1°C, although the overall width of the RTI temperature distribution is wider.

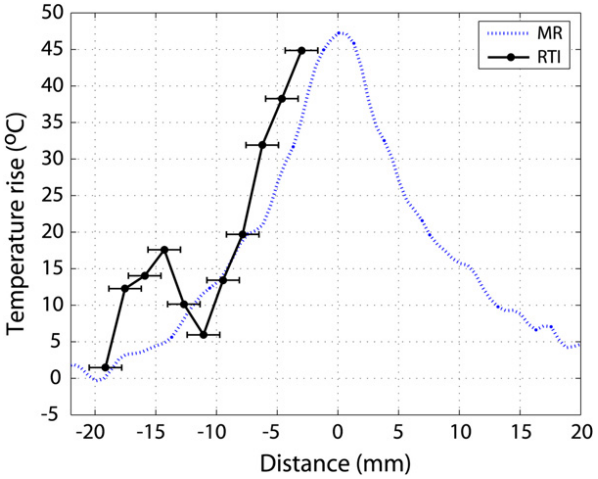


Fig. 9. Temperature rise determined from the particulate backscattering in the phantom, compared with the MR-measured temperature rise. The horizontal error bars represent uncertainty in the origin of the position at which the sound field was reflected because of the time window duration.

## DISCUSSION

The experiments performed in this study sought to evaluate ultrasonic detection of ultrasound-induced heating using a phase-contrast method. The method was previously investigated in a numerical (Clement and Hynynen 2005) and experimental (Farny and Clement 2008) study that examined the sensitivity of measuring the phase angle change from heating with a through-transmission interrogation arrangement. The current study extended those methods to a pulse-echo, or reflection mode, arrangement that is envisioned to be better suited to a clinical setup. Because of the lengthy acquisition time incurred in the measurement, tissue phantoms were used to mimic the acoustic and thermal properties of tissue. Typically, reflex transmission imaging has been based on attenuation effects along the path, but we have demonstrated that the technique has application to phase contrast effects as well.

The temperature obtained with the RTI technique agreed well with a MR thermal imaging technique, the current gold standard for noninvasive temperature

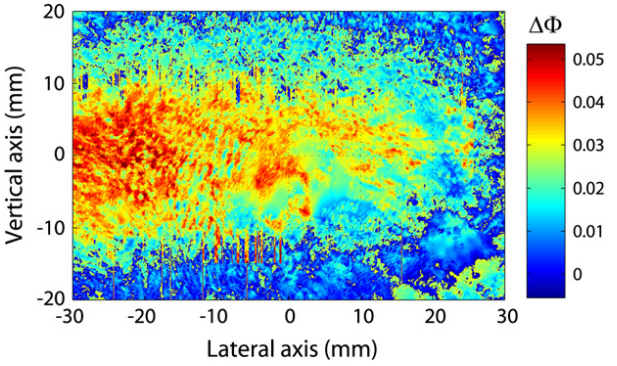


Fig. 10. RTI phase difference of heating induced with the 18% duty cycle, where the reflex transmission field was reflected off the phantom back wall.

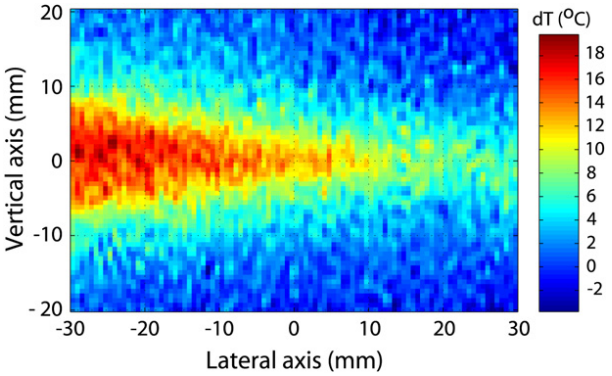


Fig. 11. MR-measured temperature rise induced with the 18% duty cycle.

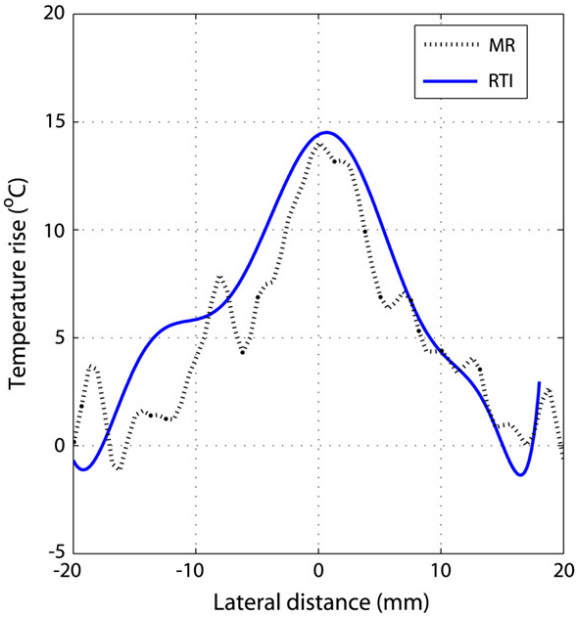


Fig. 12. Temperature rise measured at the therapy focus with the MR and RTI methods during the 18% duty cycle sonication.

measurements in tissue. For both acoustic intensities, the temperature demonstrated a similar geometric distribution and the peak temperature was within 1°C, an acceptable margin given the 3°C precision of MR thermal imaging (Germain et al. 2001; Weidensteiner et al. 2003). The temperature rise measured with the ultrasound featured a slightly wider distribution compared with the MR-derived temperature rise. Effects contributing to this discrepancy could include spatial averaging because of the MR voxel size and heat conduction incurred from the longer sonication period during the RTI scan. Alignment of the imaging transducer relative to the phantom and hydrophone may have caused non-normal reflection off the phantom back wall, leading to spreading in the detected heating. Interphantom variability may play a role, but only for the 43% duty cycle results, because the same phantom was used for both measurements that featured the 18% duty cycle sonication.

The peak temperature rise measured was 43°C, demonstrating the capability of the system for measuring over large temperature ranges, although the baseline temperature was 22°C and not body temperature. Varghese and Daniels (2004) stress the importance of the ability to measure throughout the entire temperature range that may be covered during thermal ablation procedures, potentially up to 100°C. Two issues may arise for a method that relies on the temperature dependence of sound speed in soft tissue with low fat content. First, the sound speed of such tissues only increases with temperature for a portion of the range, near an inflection temperature of 50–65°C for many tissue types, before decreasing for higher temperatures. Although our system is still in development, we believe that these problems may be overcome by our approach. By continuously tracking the phase difference within the ROI, we expect that as the inflection temperature in the hottest spot is approached, the phase difference will eventually switch polarity, indicating that the temperature has either increased beyond the inflection point, or that the spot has cooled. These two scenarios may be resolved by using heat diffusion effects to compare the temperature in this spot with the rest of the region, which will likely be cooler and will indicate the overall trend of either increased heating or cooling. Because these cooler regions will still be below the inflection temperature, the polarity of the phase difference will be unambiguous regarding the actual temperature. Anand et al. (2007, 2008) describe a similar method for resolving this issue. Monitoring the phase change dynamics after sonication will provide a final validation for this method. Second, the sound speed *contrast* near the inflection temperature is reduced for a given temperature change, because the sound speed gradient is low. Miller et al. (2002) conclude that temperatures above 50°C for many tissue types are too difficult to measure because of low sensitivity from an ultrasound echo strain measurement. As discussed above, the sensitivity of the phase contrast method is significantly higher in the presence of noise than the echo strain method, reducing the sensitivity problems encountered by Miller et al.

Both the MR and RTI images of the temperature distribution indicated that the peak temperature rise was located closer to the therapy transducer than expected (*i.e.*, not at the geometric focus). Initially, we believed the prefocal heating observed first in the RTI image was artifactual, but the shift was observed in the MR data as well, leading us to believe that the shift is the result of a lensing effect caused by the phantom and therapy transducer geometry. The phantom was cast in a cylindrical mold and the therapy transducer sonicated through the curved side of the phantom. We speculate that the

curvature of the water-phantom interface acted as an additional acoustic lens that shifted the focus closer to the therapy transducer, because the sound speed in the phantom was higher (1515 m/s) than that of the water (~1486 m/s).

A potential setback to this method is the reliance on a sufficiently strong reflection to back-project the field. Here the results relied chiefly on the reflection off the phantom back surface, which imposed a weak acoustic impedance mismatch but nonetheless presented a flat, uniform surface. However, despite their small diameter (80% between 1 and 5 $\mu$m), the backscatter off the silica particles also provided sufficient signal, to the extent that continuous spatial tracking of the temperature change was possible. It is noted that these diameters are on the order of a typical human red blood cell (6 to 8 $\mu$m), and that diagnostic ultrasound imaging often relies on weak acoustic impedance mismatches from structures much larger than the silica particles. Based on the current results, it is expected that the RTI method described here will be feasible *in vivo*, because it is likely that the SNR of the reflex transmission signal from the tissue heterogeneity will actually exceed that of the silica particles. Continuous tracking of the heat obtained from multiple reflections along the propagation axis may provide an improvement in the analysis. The results presented in Figs. 7 and 12 relied on the assumption that the temperature distribution along the imaging axis was symmetric with the distribution along the vertical axis and that the temperature rise corresponded to a Gaussian distribution. These assumptions may not hold true in an inhomogeneous medium, particularly if attenuation and conduction parameters differ along the path length. By examining the change in phase because of the position of the reflected field within the region of heating, the temperature distribution along the propagation axis will not depend on these assumptions.

The current experimental implementation introduced several limitations that should be taken into consideration. The chief barrier encountered here was speed of acquisition. Because of the lengthy hydrophone scan time, it was possible to only measure steady-state heating in tissue phantoms. The 24-h scan period may have introduced errors caused by fluctuation in water temperature from periodic environmental temperature fluctuation, spatial registration error induced by environmental vibration, and heat conduction in the phantom. In addition, the long acquisition time prevented appreciable optimization of the sonication parameters and relative positioning of the phantom and interrogation fields. Clearly, for this method to be practical, the acquisition time must be reduced dramatically. The hydrophone acquisition procedure was performed as a mock-up to an array. In practice, the diagnostic transducer and hydrophone may be replaced with a 2-D array that will both send and receive the diagnostic field. This method will require a multichannel digitization system to satisfy the Nyquist sampling criteria, although implementation of a phase-contrast filter (Pitts et al. 2001; Clement and Hynynen 2005) may allow for a significantly lower sampling rate.

A second limitation encountered here was the hydrophone, which was necessarily present in the transmitted field. Comparison of the transmitted field with and without the hydrophone and mounting wire revealed a small but detectable distortion to the diagnostic field. The impact of this effect was not immediately apparent in the phase maps, likely because of the constant change in position of the hydrophone with respect to the diagnostic field. Despite relying on the phase difference to cancel out any related effects, the back-projected field may be slightly distorted as a result. In addition, the relatively large hydrophone size was not ideal and likely contributed to spatial averaging. The poor electrical shielding of the hydrophone affected the measurement significantly, because the relative position of the two transducers, phantom and hydrophone was dictated by a relatively narrow spatial window as a result of electrical signals sensed by the hydrophone cabling when reflections off the hydrophone and phantom surface were incident on the transducer. This complication reduced the hydrophone RF signal time window that provided useful information about the reflex transmission signal. In turn, the time window imposed a restriction on the experimental arrangement for capturing the main signal of interest for this study, the reflection off the phantom back wall. This restriction is why the entire RF datastream was not available for analysis for the RTI signal (Fig. 9) based on the backscattered RF signal. Overall, the SNR also likely suffered from broadband electrical noise superimposed on the detected reflected signals. These effects would not be present for an array-based interrogation system.

Most ultrasound-based thermal imaging techniques encounter distortion as a result of thermal lensing effects, where heating along the path causes the interrogation field to self-focus (Simon et al. 1998; Miller et al. 2004; Pernot et al. 2004). As a result, a circular ripple artifact may appear in the temperature profile. These effects were apparent in some of the results obtained here as well. In Fig. 5, for example, a decrease in the heating is visible along the vertical axis at $y = 0$ mm near $x = -10$ mm. Integration of the phase difference mitigated the ripple artifacts by smoothing the effect to a certain degree, but they still adversely affected the results, because the heating effect along the vertical axis does not decrease as smoothly as expected as the lateral axis is traversed away from the therapy transducer. These ripple artifacts were compensated for along the radial $y$-axis by imposing

a Gaussian distribution for the phase change, but such a distribution would not be appropriate along the lateral *x*-axis. Compensation for this effect will be examined in future studies by introduction of refraction into the spectral projection.

As is the case with some ultrasound-based thermal imaging techniques, this method is explicitly dependent on knowledge of the sound speed dependence on temperature, a relationship that is known to vary from tissue type and is also likely to vary between subjects. One method to obtain the tissue type in a given region-of-interest could involve acquisition of a pretreatment computed tomography (CT) measurement, through which the bulk regions of fat and muscle tissue could be discerned and then applied to the RTI analysis. However, it may be possible to avoid involvement of CT by using the RTI method to identify bulk tissue types. This method would involve a pretreatment procedure, whereby a low temperature rise is induced ultrasonically in the region-of-interest and the RTI method is used to monitor the heating and cooling of the region. With the knowledge that the temperature should increase from the sonication, the direction of the phase change should reveal general trends exhibited by the tissue type. Alternately, a method for *in situ* characterization of the sound speed dependence on temperature, such as that proposed by Kaczkowski and Anand (2004), could be investigated for determining region-specific sound speed–temperature relationship, although underlying assumptions related to negligible blood flow effects, thermal lensing, and thermal conductivity spatial variability and temperature dependence would require evaluation. These approaches will be examined in future studies once an RTI array system has been developed.

Compared with current ultrasound-based thermal imaging techniques, such as cross correlation of B-mode image shifts, the method described here offers several advantages. Acquisition speed limitations notwithstanding, the projection technique allows for interrogation of the full 3-D volume within the ROI, as opposed to a 2-D image typically obtained with many speckle-tracking methods; to the best of our knowledge, Anand et al. (2007) conducted the only other study that has successfully imaged 3-D volumes, through use of a 2-D imaging array and 2-D cross correlation of the RF echo shifts. Error induced from speckle artifacts have little effect caused by the back projection step that should cause such multiple-path reflections to propagate away from the ROI. In addition, it is not anticipated that thermal expansion effects will significantly hinder the results when the temperature is based solely on its relationship to sound speed. Thermal expansion must be accounted for when the temperature dependence is related to a spatial shift (Varghese and Daniels 2004). Although the medium is still expected to undergo thermal expansion, this method relies not on tracking spatial features but on the change in sound speed through a given region, a property that should not be appreciably affected by thermal expansion. The physical scattering site off of which the heated field is reflected may be different from that used for the reference field, so long as the medium has sufficient scattering from the newly shifted medium to allow for back-projection of the backscattered field.

## CONCLUSIONS

This study has demonstrated that by applying reflex transmission imaging with back-projection techniques in a characterized medium, a 3-D temperature map may be determined. The current approach offers spatial resolution comparable to MR temperature imaging and provides several advantages compared with current ultrasound-based thermal imaging techniques. The major drawback for the present implementation is the lengthy time duration required for the measurement. This issue may be addressed with hardware improvements that we hope to pursue in the future.

*Acknowledgements*—Financial support for this research was provided by the NIH *via* Award Numbers U41, RR19703 and R25 CA089017-06A2. The authors would like to thank Dr. Nathan McDannold and Chang-Sheng Mei for assistance with the MR measurements, and Dr. P. Jason White for assistance with experimental setup.

## REFERENCES

Anand A, Savéry D, Hall C. Three-dimensional spatial and temporal temperature imaging in gel phantoms using backscattered ultrasound. IEEE Trans Ultrason Ferroelectr Freq Control 2007;54:23–31.

Anand A, Kaczkowski PJ. Noninvasive measurement of local thermal diffusivity using backscattered ultrasound and focused ultrasound heating. Ultrasound Med Biol 2008;34:1449–1464.

Bamber J, Hill C. Ultrasonic attenuation and propagation speed in mammalian tissues as a function of temperature. Ultrasound Med Biol 1979;5:149–157.

Bamber J, Nassiri D. Effect of gaseous inclusions on the frequency dependence of ultrasonic attenuation in liver. Ultrasound Med Biol 1985;11:293–298.

Clarke RL, Bush NL, Ter Haar GR. The changes in acoustic attenuation due to *in vitro* heating. Ultrasound Med Biol 2003;29:127–135.

Clement GT, Hynynen K. Ultrasound phase-contrast transmission imaging of localized thermal variation and the identification of fat/tissue boundaries. Phys Med Biol 2005;50:1585–1600.

Damianou CA, Sanghvi NT, Fry FJ, Maass-Moreno R. Dependence of ultrasonic attenuation and absorption in dog soft tissues on temperature and thermal dose. J Acoust Soc Am 1997;102:628–634.

Daniels MJ, Varghese T, Madsen EL, Zagzebski JA. Non-invasive ultrasound-based temperature imaging for monitoring radiofrequency heating—Phantom results. Phys Med Biol 2007;52:4827–4843.

Duck FA. Acoustic Properties of Tissue at Ultrasonic Frequencies. Physical Properties of Tissue. London: Academic Press; 1990.

Farny CH, Clement GT. Feasibility of ultrasound phase contrast for heating localization. J Acoust Soc Am 2008;123:1773–1783.

Germain D, Chevallier P, Laurent A, Saint-Jalmes H. MR monitoring of tumour thermal therapy. Magn Reson Mat Phys Biol Med 2001;13:47–59.

Gong X, Zhang D, Liu J, Wang H, Yan Y, Xu X. Study of acoustic nonlinearity parameter imaging methods in reflection mode for biological tissues. J Acoust Soc Am 2004;116:1819–1825.

Green PS, Arditi M. Ultrasonic reflex transmission imaging. Ultrason Imaging 1985;7:201–214.
Green PS, Ostrem JS, Whitehurst TK. Combined reflection and transmission ultrasound imaging. Ultrasound Med Biol 1991;17:283–289.
Hein I, O'Brien WS. Current time-domain methods for asserting tissue motion by analysis from reflected ultrasound echoes—A review. IEEE Trans Ultrason Ferroelectr Freq Control 1993;40:84–102.
Hindman JC. Proton resonance shift of water in the gas and liquid states. J Chem Phys 1966;44:4582–4592.
Ishihara Y, Calderon A, Watanabe H, Okamoto K, Suzuki Y, Kuroda K. A precise and fast temperature mapping using water proton chemical shift. Magn Res Med 1995;34:814–823.
Kaczkowski P, Anand A. Temperature rise measured noninvasively during thermal therapy using backscattered ultrasound. Proc 2004 IEEE Ultrason Symp 2004;1:720–723.
Kak AC, Slaney M. Principles of Computerized Tomographic Imaging. Piscataway, NJ: IEEE Press; 1988. 49–60.
King RL, Clement GT, Maruvada S, Hynynen K. Preliminary results using ultrasound transmission for image-guided thermal therapy. Ultrasound Med Biol 2003;29:293–299.
Liu X, Gong X, Yin C, Li J, Zhang D. Noninvasive estimation of temperature elevations in biological tissues using acoustic nonlinearity parameter imaging. Ultrasound Med Biol 2008;34:414–424.
Maass-Moreno R, Damianou CA, Sanghvi NT. Noninvasive temperature estimation in tissue via ultrasound echo-shifts. Part II. In vitro study. J Acoust Soc Am 1996;100:2522–2530.
McDannold N. Quantitative MRI-based temperature mapping based on the proton resonant frequency shift: Review of validation studies. Int J Hyperthermia 2005;21:533–546.
Meaney PM, Fanning MW, Paulsen KD, Lit D, Pendergrass SA, Fang Q, Moodie KL. Microwave thermal imaging: Initial in vivo experience with a single heating zone. Int J Hyperthermia 2003;19:617–641.
Miller NR, Bamber JC, Meaney PM. Fundamental limitations of noninvasive temperature imaging by means of ultrasound echo strain estimation. Ultrasound Med Biol 2002;28:1319–1333.
Miller NR, Bamber JC, ter Haar GR. Imaging of temperature-induced echo strain: Preliminary in vitro study to assess feasibility for guiding focused ultrasound surgery. Ultrasound Med Biol 2004;30:345–356.
Palussière J, Salomir R, Le Bail B, Fawaz R, Quesson B, Grenier N, Moonen CTW. Feasibility of MR-guided focused ultrasound with real-time temperature mapping and continuous sonication for ablation of VX2 carcinoma in rabbit thigh. Magn Reson Med 2003;49: 89–98.
Paulsen KD, Moskowitz MJ, Ryan TP, Mitchell SE, Hoopes PJ. Initial in vivo experience with EIT as a thermal estimator during hyperthermia. Int J Hyperthermia 1996;12:573–591.
Pernot M, Tanter M, Bercoff J, Waters KR, Fink M. Temperature estimation using ultrasonic spatial compound imaging. IEEE Trans Ultrason Ferroelectr Freq Control 2004;51:606–615.
Pitts TA, Sagers A, Greenleaf JF. Optical phase contrast measurement of ultrasonic fields. IEEE Trans Ultrason Ferroelectr Freq Control 2001; 48:1686–1694.
Quesson T, de Zwart JA, Moonen CT. Magnetic resonance temperature imaging for guidance of thermotherapy. J Magn Reson Imaging 2000;12:525–533.
Rallan D, Bush NL, Bamber JC, Harland CC. Quantitative discrimination of pigmented lesions using three-dimensional high-resolution ultrasound reflex transmission imaging. J Invest Dermatol 2007; 127:189–195.
Rieke V, Pauly KB. MR thermometry. J Magn Reson Imaging 2008;27: 376–390.
Robinson RC, Lele PP. An analysis of lesion development in the brain and in plastics by high-intensity focused ultrasound at low-megahertz frequencies. J Acoust Soc Am 1972;51:1333–1351.
Ryan LK, Foster FS. Tissue equivalent vessel phantoms for intravascular ultrasound. Ultrasound Med Biol 1997;23:261–273.
Simon C, Vanbaren P, Ebbini ES. Two-dimensional temperature estimation using diagnostic ultrasound. IEEE Trans Ultrason Ferroelectr Freq Control 1998;45:1088–1099.
Sokka SD, King R, Hynynen K. MRI-guided gas bubble enhanced ultrasound heating in in vivo rabbit thigh. Phys Med Biol 2003;48: 223–241.
Stepanishen PR, Benjamin KC. Forward and backward projection of acoustic fields using FFT methods. J Acoust Soc Am 1982;71: 803–812.
Tyreus PD, Diederich C. Two-dimensional acoustic attenuation mapping of high-temperature interstitial ultrasound lesions. Phys Med Biol 2004;49:533–546.
Varghese T, Zagzebski JA, Chen Q, Techavipoo U, Frank G, Johnson C, Wright A, Lee FT. Ultrasound monitoring of temperature change during radiofrequency ablation: Preliminary in-vivo results. Ultrasound Med Biol 2002;28:321–329.
Varghese T, Daniels MJ. Real-time calibration of temperature estimates during radiofrequency ablation. Ultrason Imaging 2004;26:185–200.
Weidensteiner C, Quesson B, Caire-Gana B, Kerioui N, Rullier A, Trillaud H, Moonen CT. Real-time MR temperature mapping of rabbit liver in vivo during thermal ablation. Magn Reson Med 2003;50:322–330.
Worthington AE, Sherar MD. Changes in ultrasound properties of porcine kidney tissue during heating. Ultrasound Med Biol 2001; 27:673–682.